SOCAR Proceedings

Fundamental Research

journal home page: http://proceedings.socar.az

TRIMETHYLOLPROPANE-BASED ALIPHATIC ESTERS: LUBRICANT PROPERTIES, BACTERICIDAL ACTIVITY AND DFT STUDY

V. M. Abbasov[1], H. N. Gurbanov[1], F. Kh. Aliyeva[1], A. M. Mammadov[1,2,3]*, A. T. Sharifov[1], R. R. Mammadova[1]

[1]*Institute of Petrochemical Processes named after Academician Y.H. Mammadaliyev, The Ministry of Science and Education of the Republic of Azerbaijan, Baku, Azerbaijan;*

[2]*Azerbaijan University of Architecture and Construction, Baku, Azerbaijan;*

[3]*Sumgayit State University, Sumgayit, Azerbaijan*

A B S T R A C T

In this research, symmetric and asymmetric aliphatic esters based on 1,1,1-trimethylolpropane (TMP) were synthesized with high yields using caproic and pelargonic acids. The synthesized compounds - TMP tricaproate (N1), TMP tripelargonate (N2), and the asymmetric dicaproate-pelargonate ester (N3) - were rigorously characterized using FT-IR and NMR (1H and 13C) spectroscopy. A comprehensive study was conducted to evaluate their physicochemical properties, viscosity-temperature characteristics, and biological activities. Experimental results demonstrated that increasing the carbon chain length leads to higher kinematic viscosity and a decrease in density; specifically, sample N2 exhibited the highest viscosity, while the asymmetric N3 ester showed a superior viscosity index of 168. These balanced tribological properties suggest that these esters are highly suitable as base stocks for high-performance, low-viscosity aviation lubricants. Furthermore, the bactericidal efficiency of the esters was evaluated against sulfate-reducing bacteria (SRB). At concentrations ranging from 25 to 100 mg/L, the compounds achieved a corrosion protection effect of 96.9-100 %, significantly outperforming standard industrial reagents. Theoretical investigations were performed using Density Functional Theory (DFT) at the B3LYP/6-31G(d,p) level to calculate HOMO (Highest Occupied Molecular Orbital) - LUMO (Lowest Unoccupied Molecular Orbital) orbitals and various quantum-chemical descriptors (ionization potential, electrophilicity index, chemical hardness, etc.). The substantial energy gaps (7.390-7.575 eV) confirm the high thermal and oxidative stability of these molecules. These theoretical findings strongly correlate with experimental data, providing a robust scientific framework for utilizing these TMP esters as next-generation lubricant components and effective multifunctional bactericidal inhibitors.

Keywords: trimethylolpropane; esters; lubricants; bactericidal activity; DFT calculations; quantum-chemical descriptors.

Date submitted: 15.09.2025 **Date accepted:** 04.05.2026 **Date published:** 01.06.2026

Introduction

The rapid advancement of modern industry and technology has imposed increasingly stringent and multifaceted requirements on lubricating materials, particularly lubricating oils. The operating conditions of mechanical systems, engines, and heavily loaded machinery are becoming progressively more demanding, which underscores the importance of high-performance lubricants capable of ensuring long-term and reliable operation. Such oils must remain stable across a wide temperature range (approximately ≥ 250 °C to -60 °C), under high pressure, and in the presence of dynamic mechanical loads. Moreover, they are expected to form a durable protective layer between frictional and contacting surfaces, thereby preventing wear, thermal degradation, and corrosion [1-6].

The development of next-generation lubricants extends beyond the improvement of conventional mineral and synthetic oils; it also requires the synthesis of novel compounds incorporating functional groups, polar centers, and reactive fragments. Of particular interest are ester-type compounds with relatively high molecular weight and a quaternary carbon atom devoid of a hydrogen atom in the β-position. Owing to their distinctive molecular architecture, such esters can deliver superior tribological performance, exhibit excellent thermal and oxidative stability, and ensure well-balanced viscosity–temperature behavior [7-10].

Synthetic esters derived from polyols and fatty acids exhibit favorable physicochemical properties for lubrication applications, even under extreme temperature conditions. In a reported study [11], esters of trimethylolpropane with C5-C18 fatty acids were synthesized and their key properties were systematically investigated. The resulting products demonstrated excellent low-temperature performance,

***E-mail:** ayazmammadov@nkpi.az

http://dx.doi.org/10.5510/OGP2026SI101185

suitable for operation in harsh environments. Moreover, as the alkyl chain length of the fatty acid increased from C5 to C18, the pour points of the esters rose from -75 °C to -42 °C, while their viscosity index increased from 80 to 208.

Beyond their tribological and physicochemical attributes, esters represent a class of compounds of particular interest due to their biological activity. The coexistence of hydrophobic aliphatic chains and polar functional groups in their molecular structures imparts surface-active properties, enabling interactions with cell membranes and influencing their structure and function [12-15]. As a result, certain esters are capable of significantly suppressing or completely inhibiting the growth of microorganisms, particularly sulfate-reducing bacteria (SRB), which are notorious for inducing corrosion in industrial systems [16-18].

Sulfate-reducing bacteria are among the principal agents of microbiologically influenced corrosion, a widespread issue in the oil, gas, and chemical industries. Their metabolic activity produces hydrogen sulfide (H_2S), which promotes equipment corrosion, degrades product quality, and may cause costly process interruptions. Conventional countermeasures typically involve the use of chemical biocides; however, many of these agents are environmentally hazardous, insufficiently effective, or require high application dosages [19-23].

Esters stand out not only for their multifunctional applications but also for their unique molecular architectures, which strongly influence their physicochemical stability, tribological behavior, as well as optical and electronic properties. Consequently, a detailed understanding of their molecular and electronic structures is essential for predicting their performance in practical applications. While experimental approaches play a crucial role, theoretical quantum-chemical methods provide a more systematic and precise framework for characterizing the properties of such compounds [24-27].

Density Functional Theory (DFT), by analyzing electron density distributions, offers valuable insights into the energetic, structural, and reactivity characteristics of complex molecular systems. Owing to its balance between computational efficiency and predictive reliability, DFT has been widely employed in the study of synthetic esters. This approach enables the determination of optimized molecular geometries, bond lengths, bond angles, torsional parameters, as well as the energies and spatial localization of HOMO and LUMO orbitals. Such descriptors provide fundamental information on molecular stability, electron-donor and electron-acceptor capacities, chemical hardness and softness, and potential reactivity pathways. In addition, DFT-derived quantum-chemical descriptors – including ionization potential, electron affinity, chemical potential, and electrophilicity index – serve as a theoretical basis for explaining the physicochemical behavior of esters, their viscosity-temperature stability under tribological conditions, and their biological (e.g., bactericidal) activity mechanisms [24, 28-32].

In the present work, symmetric and asymmetric esters of 1,1,1-trimethylolpropane with caproic and pelargonic acids were synthesized. Their physicochemical properties, bactericidal activity against sulfate-reducing bacteria, and molecular structures were investigated using IR and NMR spectroscopic methods. In parallel, DFT calculations were employed to obtain optimized molecular geometries, bond lengths, HOMO-LUMO orbital energies, and quantum-chemical descriptors, thereby providing theoretical insights into their properties and potential applications.

Experimental section

All reagents and solvents were obtained from Sigma-Aldrich and used without further purification. 1H and 13C NMR spectra were recorded at 20 °C on a Bruker Fourier 300 MHz spectrometer using tetramethylsilane (TMS) as the internal standard, deuterated chloroform ($CDCl_3$) and benzene (C_6D_6) as the solvents. Infrared (IR) spectra were collected in the range of 600-4000 cm^{-1} with a BRUKER LUMOS FT-IR microscope spectrometer. The acid numbers of the synthesized compounds were determined in accordance with GOST 5985-79. Kinematic viscosities at 40 °C and 100 °C were measured following the procedure specified in GOST 33-2000.

Symmetric and asymmetric esters of TMP with aliphatic monocarboxylic acids were synthesized, and three ester samples obtained with caproic and pelargonic acids were investigated.

Synthesis of the symmetric TMP caproate ester. The synthesis was carried out in a three-necked round-bottom flask equipped with a mechanical stirrer, thermometer, reflux condenser, and Dean-Stark water separator.

The reaction mixture consisted of 0.2 mol TMP (CAS 77-99-6), 0.64 mol caproic acid (CAS 142-62-1), and 1 wt% of the total mixture of the "Seokar-2" catalyst. To this, 50 mL of toluene was added as the solvent, and the mixture was heated. The progress of the reaction was monitored by the volume of separated water and the acid number of the mixture. Upon completion, toluene was removed under atmospheric pressure, and the product was distilled under vacuum at 170–180 °C/2 mmHg. The isolated yield of the

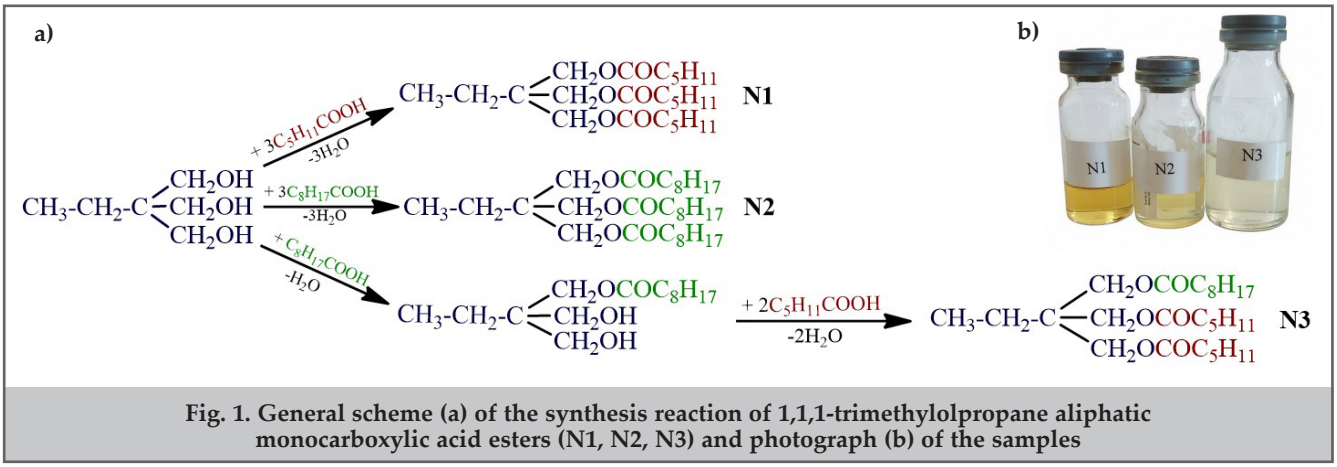

Fig. 1. General scheme (a) of the synthesis reaction of 1,1,1-trimethylolpropane aliphatic monocarboxylic acid esters (N1, N2, N3) and photograph (b) of the samples

ester was 90% of the theoretical value.

Synthesis of the symmetric TMP pelargonate ester. The procedure was analogous to that described above for the caproate ester.

The overall synthetic route for the symmetric (N1, N2) and asymmetric (N3) esters of TMP with caproic and pelargonic acids is presented in figure 1.

Synthesis of the asymmetric TMP ester (N3). The synthesis was carried out in two steps. In the first step, TMP was esterified with pelargonic acid at a molar ratio of 1:1 in the presence of toluene until the calculated amount of water was collected. In the second step, caproic acid was introduced into the reaction mixture in a molar ratio of 1:2.2 relative to TMP. The completion of the reaction was determined by the volume of water collected and the acid number.

The esterification of TMP with aliphatic acids thus yielded three esters with different chain lengths: N1 – the symmetric tricaproate ester, N2 – the symmetric tripelargonate ester, and N3 – the asymmetric caproate-pelargonate ester.

Results and discussion

The physicochemical and viscosity-temperature properties of the synthesized TMP esters were determined, and the data are summarized in table 1.

As seen from table 1, an increase in the number of carbon atoms in the side chain results in a decrease in density (from 0.9772 for N1 to 0.9479 for N2), while the refractive index slightly increases (from 1.4484 to 1.4567). The asymmetric ester N3 exhibits intermediate values.

With respect to viscosity-temperature behavior, N2 displayed the highest kinematic viscosity at both 40 °C (22.39 mm²/s) and 100 °C (4.82 mm²/s). N3 exhibited intermediate values (16.20 and 4.14 mm²/s, respectively), whereas N1 showed the lowest viscosity (12.82 and 3.29 mm²/s).

The viscosity index (VI) also increased with the length of the fatty acid chain: 129 for N1 and 142 for N2. Remarkably, the asymmetric ester N3, due to the disruption of molecular symmetry, exhibited the highest VI value of 168. Based on these viscosity-temperature characteristics, the synthesized esters can be recommended as potential candidates for use in low-viscosity aviation lubricants.

Bactericidal activity

The bactericidal activities of the symmetric and asymmetric TMP esters against SRB were investigated, and the results are presented in table 2.

The results in table 2 demonstrate that the synthesized esters N1, N2, and N3 exhibit strong antibacterial effects against SRB, with efficacy increasing with concentration. At concentrations as low as 25 mg/L, the bactericidal effect

Table 1

Physicochemical and viscosity-temperature properties of TMP esters (N1, N2, N3)

Sample	Acid value, mgKOH/g	d_4^{20}	n_D^{20}	Kinematic viscosity, mm²/s		Viscosity index
				100 °C	40 °C	
N1	neutral	0.9772	1.4484	3.29	12.82	129
N2	neutral	0.9479	1.4567	4.82	22.39	142
N3	neutral	0.9692	1.5213	4.14	16.20	168

Table 2

Bactericidal activity of symmetric and asymmetric TMP esters against SRB

Sample	Concentration (mg/L)	Bacterial count (cells/mL)	H_2S content (mg/L)	Bactericidal effect (%)
N1	25	10^1	11.3	96.9
	50	-	-	100
	100	-	-	100
N2	25	-	7.1	98.1
	50	-	-	99.2
	100	-	-	100
N3	25	-	-	100
	50			
	100			
Control I: *H_2S content in SRB-free medium*	24 mg/L			
Control II: *H_2S content in SRB-containing medium*	375 mg/L			
Control-III: *bacterial count in nutrient medium*	10^8 cells/mL			
AMDOR-IK-7	50	-	-	60
	100	-	-	75
AMDOR-IK-10	50	-	-	40
	100	-	-	80

exceeded 95%. At 50 mg/L, nearly complete inhibition (≈99%) was observed, and at 100 mg/L, all esters achieved full bactericidal activity (100%), completely suppressing bacterial growth and H_2S production.

For comparison, industrial reagents AMDOR-IK-7 and AMDOR-IK-10 displayed significantly lower efficiencies under the same conditions. This highlights the superior performance of the synthesized esters and supports their potential application as alternative bactericidal inhibitors in industrial practice.

Overall, the analysis confirms that all three esters possess high antibacterial potential, with N2 showing the strongest effect even at lower concentrations.

Structural characterization

The structures of the synthesized esters were confirmed by IR and NMR spectroscopy. Representative spectra supporting these findings are presented in figures 2-5.

N1. The FTIR spectrum of N1 (fig. 2a) shows deformation vibrations of C–H bonds from CH_3 and CH_2 groups at 733, 1382, 1418, and 1464 cm^{-1}. Stretching vibrations of C–H bonds appear at 2872, 2931, and 2957 cm^{-1}. The C–O bond stretching of the ester is detected between 1097–1157 cm^{-1}, and a prominent band at 1736 cm^{-1} corresponds to the ester carbonyl (C=O) stretching.

N2. In the spectrum of N2 (fig. 2b), the CH_3 and CH_2 groups exhibit bending vibrations at 723, 1381, 1418, and 1464 cm^{-1}. C–H stretching is observed at 2854, 2924, and 2955 cm^{-1}. The ester C–O stretch appears at 1106 and 1152 cm^{-1}, while the ester carbonyl stretching is indicated by the strong band at 1738 cm^{-1}.

N3. FTIR analysis of N3 (fig. 2c) reveals bending vibrations of C–H bonds for CH_3 and CH_2 groups at 725, 1382, 1418, and 1464 cm^{-1}. The stretching vibrations of C–H are recorded at 2856, 2926, and 2956 cm^{-1}. The ester C–O stretching is evident at 1103 and 1154 cm^{-1}, and the carbonyl group (C=O) shows a strong absorption at 1737 cm^{-1}.

DFT study

The theoretical investigation of the synthesized TMP esters was performed within the framework of density functional theory. Geometrical optimizations were carried out using the B3LYP functional in combination with the 6-31G(d,p) basis set, and all calculations were conducted using the ORCA 4.2.1 software package [33].

Based on the optimized structures, a series of quantum-chemical descriptors characterizing the electronic structure of the molecules were calculated. These included the energies of the highest occupied molecular orbital (EHOMO) and the lowest unoccupied molecular orbital (ELUMO), chemical hardness and softness, electronegativity, chemical potential, electrophilicity index, ionization potential, and electron affinity. These parameters provide insight into the molecules' reactivity, electron-donating and electron-accepting capabilities, and, in addition to their physicochemical stability, establish a theoretical basis for predicting viscosity-temperature stability relevant to lubricant applications, as well as potential bactericidal mechanisms.

Figure 6 illustrates the optimized geometries of the TMP esters (N1, N2, N3).

Based on the optimized structures, all three TMP esters exhibit classical resonance within the ester fragment. The

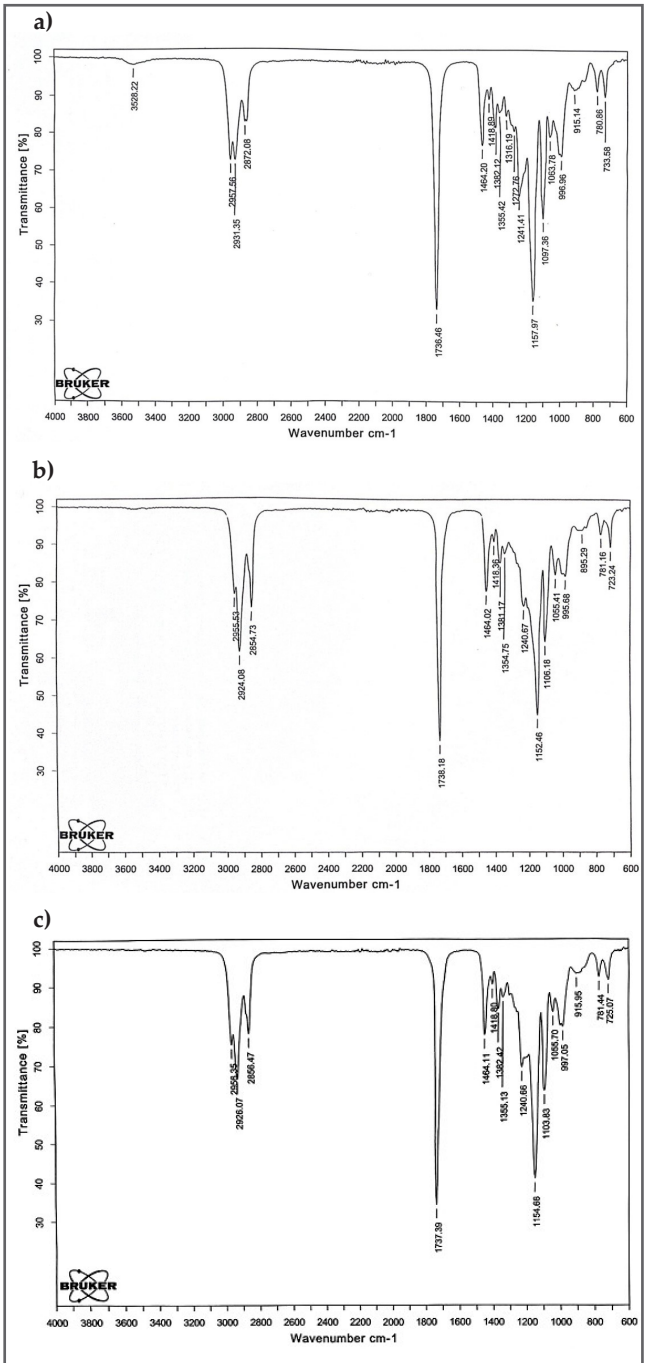

Fig. 2. FT-IR spectra of N1 (a), N2 (b), and N3 (c) samples

carbonyl C=O bond is relatively short, the acyl-side C–O bond is moderately short, and the alkoxy-side C–O bond is longer. The bond lengths correspond to typical ranges indicated in the figure: C=O ~1.20-1.22 Å, acyl C–O 1.33-1.36 Å, alkoxy C–O 1.43-1.46 Å, and aliphatic C–C ~1.52–1.54 Å. This pattern is preserved across N1, N2, and N3, with minor variations (≈0.005-0.015 Å) arising from chain length and asymmetry.

At the central junction, the proximity of the three ester arms allows for weak C–H···O interactions, primarily stabilizing the electron density associated with the alkoxy C–O bonds and accommodating slight elongations of these bonds. In symmetric structures (N1, N2), these weak interactions are more evenly distributed, partially compensating intramolecular dipole moments. In contrast, the asymmetry in N3 prevents full compensation, leading to a modest increase in the overall dipole moment. This observation correlates with minor shifts in carbonyl positions and subtle

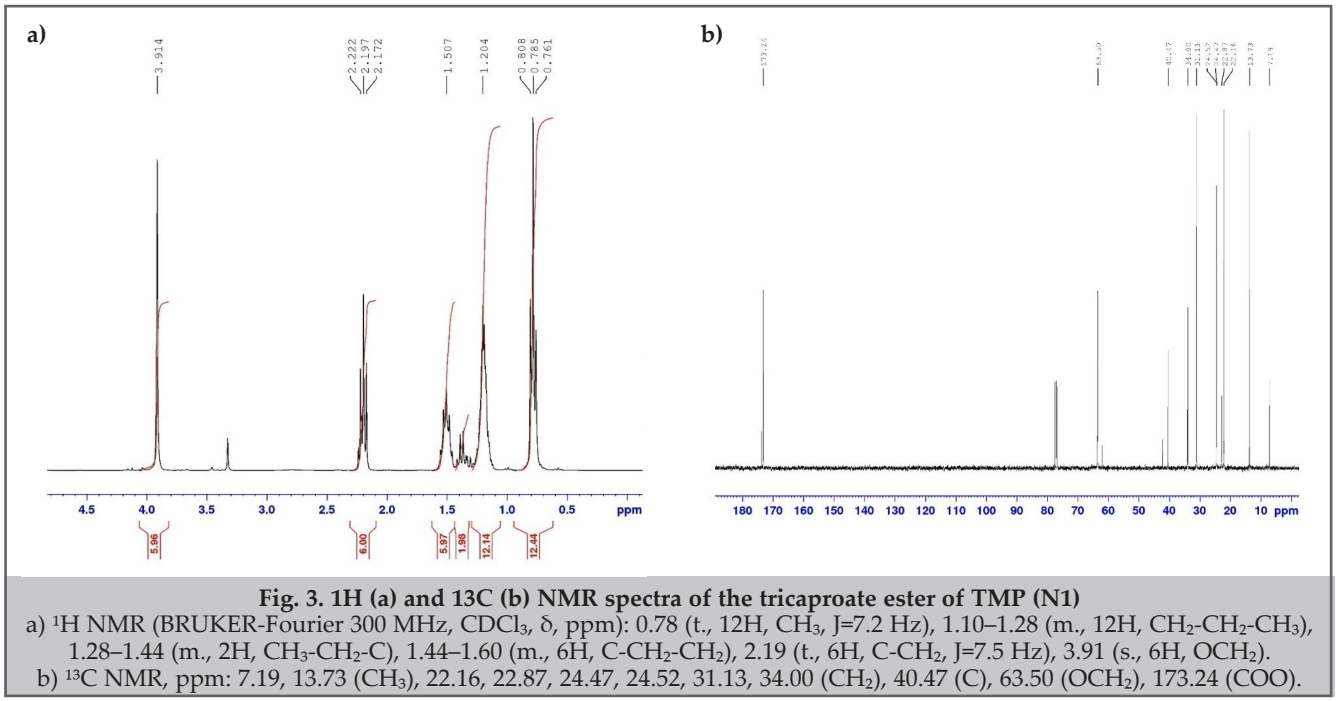

Fig. 3. 1H (a) and 13C (b) NMR spectra of the tricaproate ester of TMP (N1)
a) ^{1}H NMR (BRUKER-Fourier 300 MHz, $CDCl_3$, δ, ppm): 0.78 (t., 12H, CH_3, J=7.2 Hz), 1.10–1.28 (m., 12H, CH_2-CH_2-CH_3), 1.28–1.44 (m., 2H, CH_3-CH_2-C), 1.44–1.60 (m., 6H, C-CH_2-CH_2), 2.19 (t., 6H, C-CH_2, J=7.5 Hz), 3.91 (s., 6H, OCH_2).
b) ^{13}C NMR, ppm: 7.19, 13.73 (CH_3), 22.16, 22.87, 24.47, 24.52, 31.13, 34.00 (CH_2), 40.47 (C), 63.50 (OCH_2), 173.24 (COO).

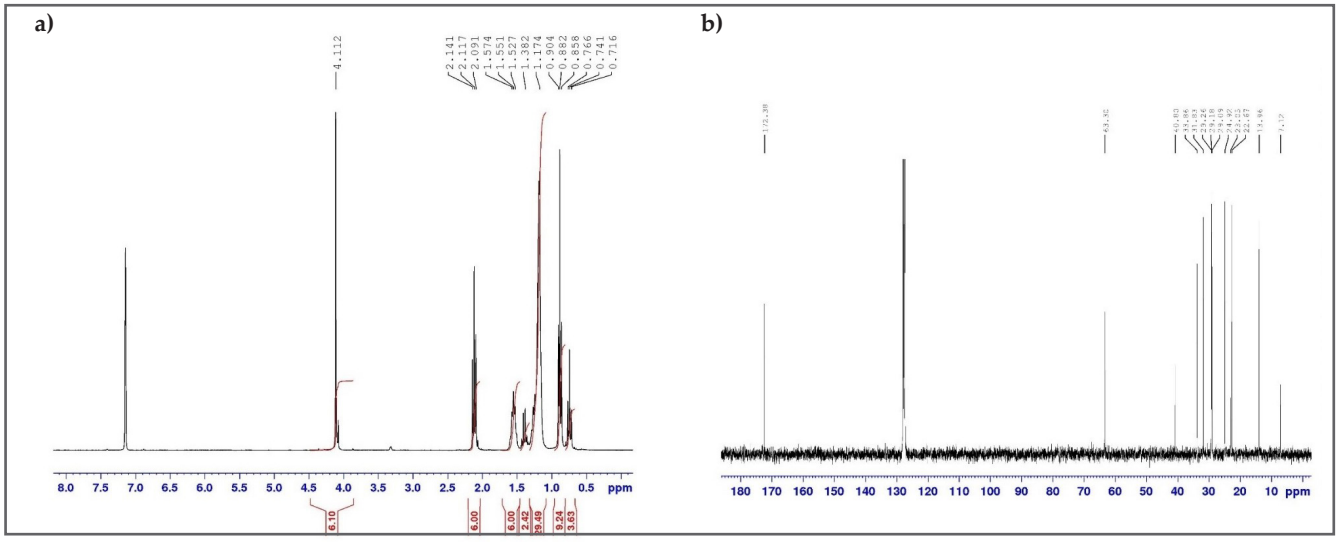

Fig. 4. 1H (a) and 13C (b) NMR spectra of the tripelargonate ester of TMP (N2)
a) ^{1}H NMR (BRUKER-Fourier 300 MHz, C6D6, δ, ppm): 0.74 (t., 3H, CH_3, J=7.5 Hz), 0.88 (t., 9H, CH_3, J=7.2 Hz), 1.11-1.31 (m., 30H, CH_2-CH_2-CH_2-CH_2-CH_2-CH_3), 1.31-1.49 (m., 2H, CH_3-CH_2-C), 1.49-1.61 (m., 6H, C-CH_2-CH_2), 2.12 (t., 6H, C-CH_2, J=7.8 Hz), 4.11 (s., 6H, OCH_2); b) ^{13}C NMR, ppm: 7.12, 13.96 (CH_3), 22.67, 23.05, 24.92, 29.09, 29.18, 29.26, 31.83, 33.86 (CH_2), 40.80 (C), 63.30 (OCH_2), 172.38 (COO)

chemical shifts in methylene/methine 1H/13C NMR signals.

In summary, the shorter C=O and slightly longer acyl C–O bonds in N2 account for a stronger "double-bond" character of the carbonyl group, which, combined with enhanced dispersion due to long chains, increases viscosity. In N1, the shorter chains result in more "resonance-like" bond lengths, promoting lower viscosity. N3, with mixed chain lengths and asymmetry, exhibits intermediate bond lengths and spectral-physical properties, reflecting somewhat weaker packing and partially elevated polarity.

Figure 7 illustrates the HOMO and LUMO orbitals for N1, N2, and N3, highlighting electronic distribution and potential reactivity sites.

Analysis of the molecular orbitals obtained from DFT calculations reveals that, in all three esters, the HOMO is predominantly localized near the ester functional groups. Specifically, the HOMO density is concentrated on the carbonyl oxygen and partially delocalized along the carbonyl π-system. In symmetric structures (N1 and N2), the HOMO exhibits greater delocalization, evenly distributed across all carbonyl oxygens, whereas in the asymmetric ester (N3), the HOMO is more localized on a single carbonyl group. This asymmetric distribution results in uneven electron density within the molecule and may enhance site-specific reactivity.

The LUMO, in all cases, corresponds to the π* orbital of the carbonyl group and is primarily localized on the carbonyl carbons. These orbitals define the regions susceptible to electrophilic attack. In N1 and N2, the LUMO is delocalized over all carbonyl carbons, indicating balanced electron-accepting regions in the symmetric molecules. In contrast, the LUMO in N3 is predominantly concentrated on one carbonyl group, suggesting increased susceptibility of this site to electrophilic interactions.

Overall, the HOMO and LUMO distributions indicate that

the electronic density of these TMP esters is largely centered on the ester functional groups. The alkyl chains show minimal participation in either HOMO or LUMO orbitals; their role is primarily to provide a hydrophobic environment and modulate the physicochemical properties of the molecules. Symmetric esters exhibit broader orbital delocalization, reflecting enhanced stability and balanced electronic distribution, while the asymmetric ester demonstrates localized orbitals that may confer higher selectivity in reactivity and more anisotropic electronic behavior.

Based on literature reports [24, 34-37], various quantum-chemical parameters for the studied esters were calculated and are summarized in table 3.

HOMO – highest occupied molecular orbital
LUMO – lowest unoccupied molecular orbital
Eg – HOMO-LUMO gap
IP – ionization potential
EA - electron affinity
μ – chemical potential
η – chemical hardness
S – chemical softness
ω – electrophilicity index
λ_{onset} – approximate absorption onset

The calculated HOMO and LUMO energies provide insight into the electronic structure and reactivity of the TMP esters. For N1, E_{HOMO} = -7.094 eV and E_{LUMO} = 0.304 eV, resulting in a HOMO-LUMO gap of 7.398 eV, indicating that the molecule is electronically rigid and exhibits relatively low reactivity. For N2, E_{HOMO} = -7.210 eV, E_{LUMO} = 0.365 eV, and the gap is 7.575 eV, suggesting slightly higher electronic rigidity and enhanced oxidative stability compared to N1 and N3. N3 exhibits values close to N1 with E_{HOMO} = -7.086 eV, E_{LUMO} = 0.304 eV, and a gap of 7.390 eV.

The ionization potential (IP = $-E_{HOMO}$) reflects the resistance of molecules to electron loss. Calculated IPs follow the order N2 > N1 ≈ N3, indicating that N2 is slightly more resistant to electron removal. Electron affinity ($E_A \approx -E_{LUMO}$) represents the tendency of molecules to accept electrons; all esters show negative EA values, suggesting low propensity for spontaneous electron uptake. The chemical potential (μ) and hardness (η) characterize the balance of electron-donating and electron-accepting capabilities and the overall reactivity of the molecules. The computed μ values range from -3.39 to -3.42 eV, and η ranges from 3.695 to 3.788 eV, indicating that the molecules are moderately hard and stable.

The electrophilicity index ($\omega \approx \mu^2/2\eta$) estimates the ability of a molecule to accept electrons. Values for N1-N3 are approximately 1.55-1.56 eV, indicating moderate electrophilic character. The estimated optical absorption onset ($\lambda_{onset} \approx 1240/Eg$) lies in the range of 163–168 nm, suggesting transparency in the visible region and high photostability [38-42].

These quantum-chemical descriptors provide critical insights into the physicochemical and tribological properties of the esters. The large HOMO–LUMO gap and high hardness contribute to oxidative and thermal stability, which is essential for long-term performance as lubricants. The electrophilicity index and chemical potential are useful for predicting potential bactericidal activity and evaluating possible interactions with biomembranes and other biomolecules. Overall, these calculated parameters establish a theoretical foundation connecting molecular electronic structure to practical application potential.

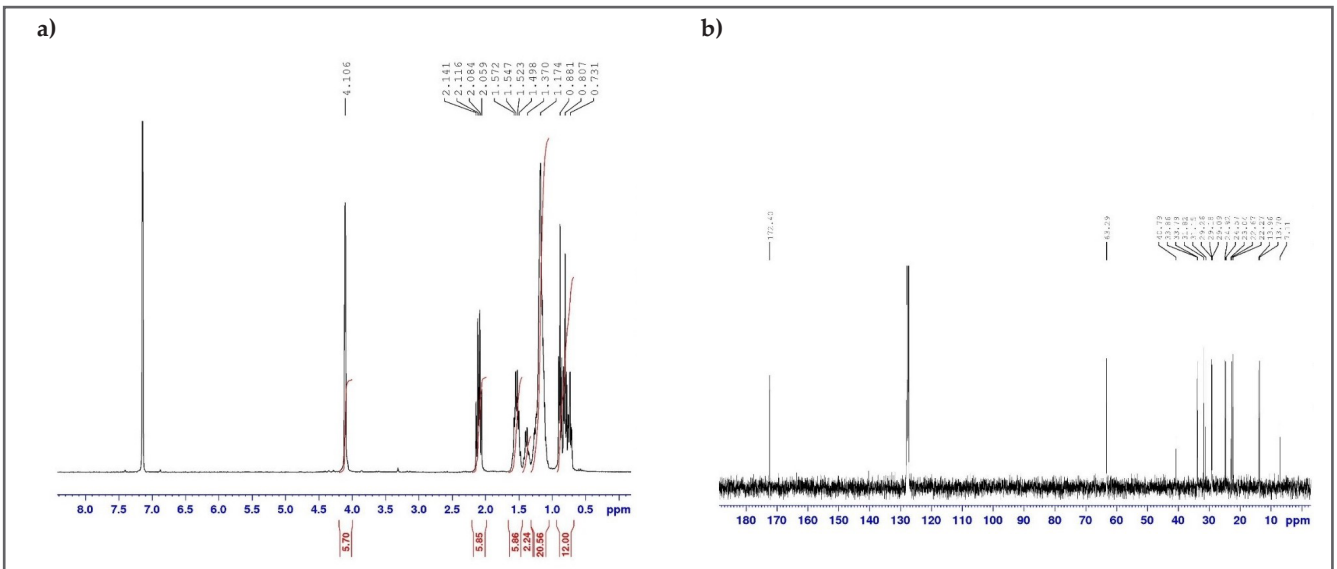

Fig. 5. 1H (a) and 13C (b) NMR spectra of the asymmetric caproate–pelargonate ester of TMP (N3)
a) ^{1}H NMR (BRUKER-Fourier 300 MHz, C6D6, δ, ppm): 0.67-0.91 (m., 12H, CH_3), 1.09-1.31 (m., 18H, CH_2), 1.31-1.48 (m., 2H, CH_3-CH_2-C), 1.48-1.63 (m., 6H, C-CH_2-CH_2), 2.05-2.15 (m., 6H, C-CH_2), 4.10 (s., 6H, OCH_2).
b) ^{13}C NMR, ppm: 7.11, 13.70, 13.96 (CH_3), 22.27, 22.67, 23.04, 24.57, 24.92, 29.09, 29.18, 29.26, 31.15, 31.82, 33.79, 33.86 (CH_2), 40.79 (C), 63.29 (OCH_2), 172.40 (COO).

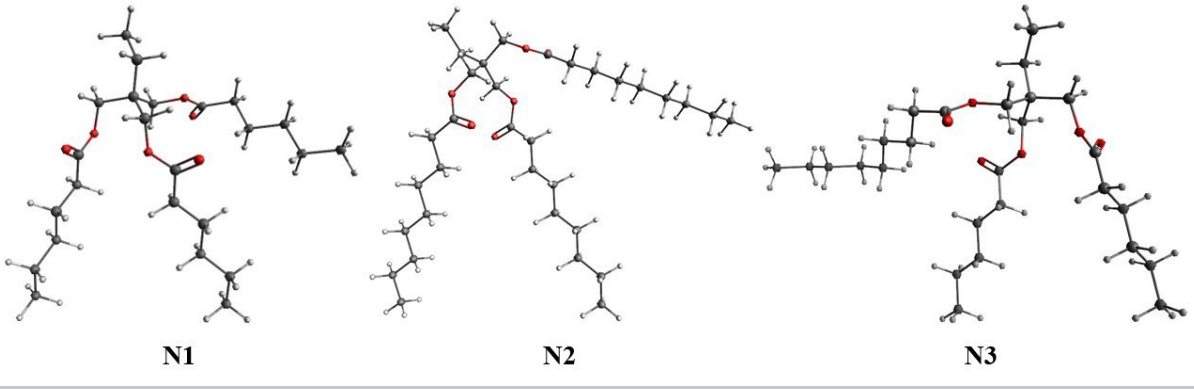

Fig. 6. Optimized geometries of TMP esters (N1, N2, N3)

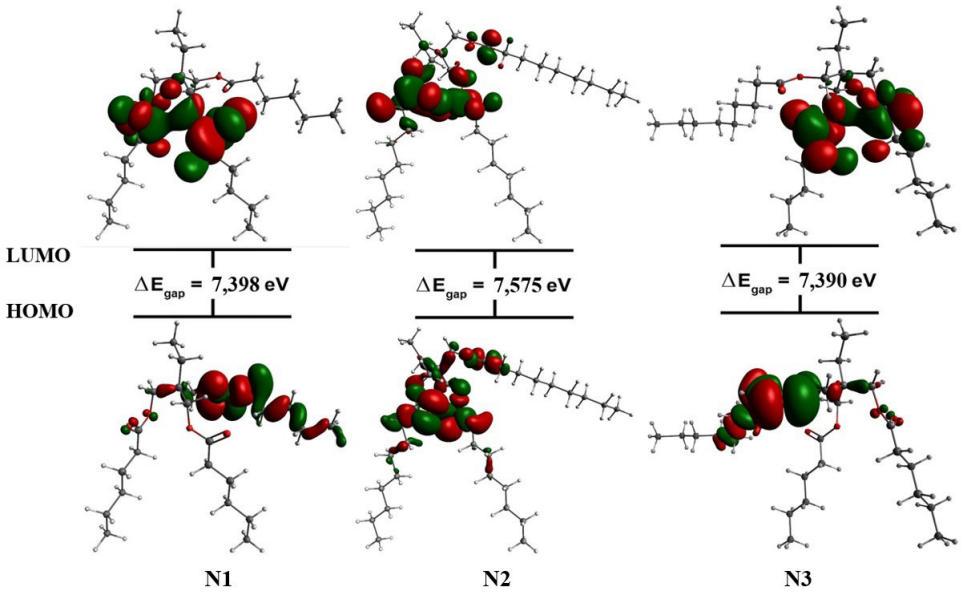

Fig. 7. HOMO and LUMO orbitals of TMP esters (N1, N2, N3)

Conclusions

Symmetric and asymmetric TMP esters with aliphatic monocarboxylic acids were successfully synthesized, and their physicochemical, viscosity-temperature, and bactericidal properties were investigated. The synthesized esters - N1 (tricapron ester), N2 (tripelargon ester), and N3 (capron-pelargon mixed ester) - exhibited distinct densities, refractive indices, and viscosity characteristics. Based on viscosity-temperature behavior, these esters are suitable as low-viscosity aviation oils.

Bactericidal tests demonstrated that all three esters exhibited strong protective effects against SRB, with 96.6-100% efficacy at 25 mg/L and complete bactericidal activity at 100 mg/L. IR and NMR analyses confirmed the structures of the esters, and DFT calculations demonstrated their high stability, resistance to oxidation, and thermal robustness.

TMP-based esters show promise as multifunctional additives, serving both as lubricant components and potential bactericidal agents, highlighting their broad application potential in industrial settings.

References

1. Yao, T., Zhang, N., Hu, J., et al. (2020). Effect of temperature on the chemical composition and physicochemical properties of diester aviation lubricating oil. *International Journal of Chemical Engineering*, 2020, 8829206.

2. Xie, M., Xu, D., Shen, J., Zhang, C. (2024). Achieving the good thermal-stability and lubricity via a dihydroxy biolubricant from the agro-waste of Codonopsis pilosula. *Renewable Energy*, 221(C), 119867.

3. Bakunin, V. N., Parenago, O. P. (1992). A mechanism of thermo-oxidative degradation of polyol ester lubricants. *Journal of Synthetic Lubrication*, 9(2), 127–143.

4. Rozga, P., Beroual, A., Przybylek, P., et al. (2020). A review on synthetic ester liquids for transformer applications. *Energies*, 13(23), 6429.

5. Esipovich, A. L., Kanakov, E. A., Charykova, T. A., et al. (2024). A comprehensive study on physicochemical properties of fatty acid esters derived from different vegetable oils and alcohols and their potential application. *Energies*, 17(24), 6407.

6. Hu, C., Ai, J., Ma, L., et al. (2021). Ester oils prepared from fully renewable resources and their lubricant base oil properties. *ACS Omega*, 6(25), 16343–16355.

7. Gurbanov, H. N., Abdullayeva, M. M., Yusifova, L. M. (2024). Synthesis of complex esters of 1,1,1-trimethylolpropane and research of them as high temperature resistant lubricants. *Processes of Petrochemistry and Oil Refining*, 25(2), 419-425.

8. Kamyab, B., Beims, R. F., Chio, C., et al. (2024). Synthesis of TMP esters as a biolubricant from canola oil via a two-step transesterification–transesterification process. *Canadian Journal of Chemical Engineering*, 102(1), 35–52.

9. Mammadyarov, M. A., Gurbanov, H. N., Yusifova , L. M. (2021). Creation of new oil compositions based on complex esters of cyclic and alyphatic neopolyols and alkylbenzene carbohydrogen oils. P*roceedings of the Azerbaijan National Academy of Sciences*, 1-2, 19-23.

10. Mammadyarov, M. A., Aliyeva, F. Kh., Gurbanov, G. N. (2017). Sinteticheskiye smazochniye masla (struktura i svoystva). *Moscow: Nauchniy Mir*.

11. Åkerman, C. O. C., Gaber, Y., Abd Ghani, N., et al. (2011). Clean synthesis of biolubricants for low temperature applications using heterogeneous catalysts. *Journal of Molecular Catalysis B: Enzymatic*, 72, 263–269.

12. Firstova, A. A., Kofanov, E. R., Kovaleva, M. I. (2023). Synthesis and biological activity of esters based on cycloalkenedicarboxylic acids. *Russian Journal of Bioorganic Chemistry*, 49, 65–75.

13. Vassilev, D. S., Petkova, N. T., Tumbarski, Y., et al. (2020). Application of the principles of "green chemistry" for the synthesis of 10-undecylenic aliphatic esters with antimicrobial activity. *Journal of Renewable Materials*, 8(6), 675–686.

14. Campana, R., Merli, A., Verboni, M., et al. (2019). Synthesis and evaluation of saccharide-based aliphatic and aromatic esters as antimicrobial and antibiofilm agents. *Pharmaceuticals*, 12(4), 186.

15. Shaaban, M. T., Ghaly, M. F., Fahmi, S. M. (2021). Antibacterial activities of hexadecanoic acid methyl ester and green-synthesized silver nanoparticles against multidrug-resistant bacteria. Journal of Basic Microbiology, 61(6), 557–568.

16. Aliyeva, F. Kh., Aghamaliyeva, D. B., Israfilova, K. O. (2024). Study of esters of (C_3–C_{10}) dicarboxylic acids as effective bactericide-inhibitors. *Processes of Petrochemistry and Oil Refining*, 25(4), 1002-1007.

17. Aliyeva, F. Kh., Aghamaliyeva, D. B., Israfilova, K. O. (2025). Dicarboxylic acid esters as bactericidal inhibitors against corrosion. *AZ Patent İ 2024 0029.*

18. Aliyeva, F. Kh., Aghamaliyeva, D. B., Israfilova, K. O. (2023). Diesters of malonic acid as bactericidal inhibitors against corrosion. *AZ Patent İ 2023 0095.*

19. Gao, G., Wang, J., Liang, P., et al. (2024). Two novel triazine-based quaternary ammonium salt Gemini surfactants as potential corrosion inhibitors for carbon steel in a sulfate-reducing bacteria solution: Experimental and theoretical studies. *Heliyon*, 10(23), e40385.

20. Asadov, Z. H., Ahmadova, G. A., Rahimov, R. A., et al. (2018). Effect of spacer nature on surface properties of new counterion coupled gemini surfactants based on dodecyldiisopropylol amine and dicarboxylic acids. *Colloids and Surfaces A: Physicochemical and Engineering Aspects*, 550, 115-122.

21. Mammadov, A. M. (2021). Synthesis of imidazole-based complexes and investigation of their bactericidal properties against SRB. *Processes of Petrochemistry and Oil Refining*, 22(4), 537–545.

22. Asadov, Z. H., Agamaliyeva, D. B., Ahmadova, G. A., et al. (2019). Micellization and adsorption properties of new cationic gemini surfactants having hydroxyisopropyl group. *Journal of Chemical & Engineering Data*, 64(3), 952–962.

23. Mammadov, A. M., Abbasov, V. M., Jafarova, R. A., et al. (2025). Inhibitory-bactericidal properties of phenyldiazenylphenyl-containing phenanthroimidazoles and DFT calculations. *Bulletin of the Russian Academy of Sciences: Physics*, 89, 1619–1625.

24. Martínez-Cifuentes, M., Soto-Tapia, E., Linares-Pipón, C., et al. (2023). Design of β-keto esters with antibacterial activity: Synthesis, in vitro evaluation, and theoretical assessment of their reactivity and quorum-sensing inhibition capacity. *Pharmaceuticals*, 16(10), 1339.

25. Wang, Y., Lin, X., Wang, M., Wang, J. (2021). A DFT study on the molecular properties of synthetic ester under the electric field. *Open Physics*, 19(1), 647–656.

26. Kawsar, S. M. A., Hosen, M. A., Fujii, Y., Ozeki, Y. (2020). Thermochemical, DFT, molecular docking and pharmacokinetic studies of methyl β-D-galactopyranoside esters. *Journal of Computational Chemistry and Molecular Modeling*, 4(4), 10663.

27. Qamar, S., Perveen, F., Akhter, Z., et al. (2022). 4,4-Nitrophenoxyaniline derived azo ester: Structural elucidation, DFT simulation, and DNA interactional studies via wet and in silico methods. *Journal of Molecular*

Structure, 1250 (Part 2), 131695.

28. Qamar, S., Perveen, F., Akhter, Z., et al. (2022). 4,4-Nitrophenoxyaniline derived azo ester: Structural elucidation, DFT simulation, and DNA interactional studies via wet and in silico methods. *Journal of Molecular Structure*, 1250(Part 2), 131695.

29. Yolchuyeva, U. J., Abbasov, V. M., Abbasov, O. R., et al. (2026). N-octylaminopropan-2-ol surfactant for crude-oil asphaltene dispersion: Integrated experimental and modeling insights. *Fuel*, 404 (Part B), 136286.

30. Abbasov, V. M., Alimadatli, N. Y., Azizov, R. E., et al. (2023). Synthesis of complexes of oleic acid with alkylamines and theoretical study of their structures. *Processes of Petrochemistry and Oil Refining*, 4(24), 831–842.

31. Yolchuyeva, U. J., Abbasov, V. M., Jafarova, R., et al. (2024). Chemical composition and molecular structure of asphaltene in Azerbaijani crude oil: A case study of the Zagli field. *Fuel*, 373, 132084.

32. Abdullayev, Y., Mammadov, A., Karimova, N., et al. (2020). Construction of new azo-group containing polycyclic imidazole derivatives: Computational mechanistic, structural, and fluorescence studies. *ChemistrySelect*, 5, 6224–6229.

33. Neese, F. (2011). The ORCA program system. Wiley Interdisciplinary Reviews: *Computational. Molecular Science*, 2(1), 73–78.

34. Oyewole, R. O., Oyebamiji, A. K., Semire, B. (2020). Theoretical calculations of molecular descriptors for anticancer activities of 1,2,3-triazole-pyrimidine derivatives against gastric cancer cell line (MGC-803): DFT, QSAR and docking approaches. *Heliyon*, 6(5), e03926.

35. Abbasov, V. M., Orujova, N. S., Jafarova, R. A., et al. (2024). Synthesis and theoretical calculations of 4[4,5-diphenyl-1-(4-(phenyldiazenyl)phenyl)-1H-imidazol-2-yl]-phenol. *Processes of Petrochemistry and Oil Refining*, 25(1), 89–97.

36. Aliyeva, F. Kh., Mammadov, A. M., Mammadova, G. F., Isayev, N. Z. (2025). DFT study of alkenyl succinic anhydrides. *Processes of Petrochemistry and Oil Refining*, 26(2), 614–623.

37. Guerguer, F., Rossafi, B., Abchir, O., et al. (2025). Potential Azo-8-hydroxyquinoline derivatives as multi-target lead candidates for Alzheimer's disease: An in-depth in silico study of monoamine oxidase and cholinesterase inhibitors. *PLOS One*, 20(1), e0317261.

38. Ustunel, H., Toffoli, D. (2022). Tribology at the atomic scale with density functional theory. *Electronic Structure*, 4(2), 023002.

39. Wang, Y., He, M., He, W., et al. (2022). The influences of atom relaxation on the DFT-calculated friction properties of the h-BN/h-BN and Gr/Gr interfaces. *Tribology International*, 173, 107586.

40. Abbasov, V. M., Abuzarzada, A. H., Mammadov, A. M., et al. (2024). Study of the nitration reaction of 1-octene and DFT calculations. *Processes of Petrochemistry and Oil Refining*, 25(4), 985–993.

41. Orujova, N. S., Abbasov, V. M., Jafarova, R. A., et al. (2025). In vitro, in silico, and DFT evaluation of antimicrobial imidazole derivatives with insights into mechanism of action. *Scientific Reports*, 15, 37723.

42. Abbasov, V. M., Mammadov, A. M., Azizov, R. E., et al. (2025). Green synthesis and DFT calculations of 4'-(2-phenyl-1H-phenanthro[9,10-d]imidazol-1-yl)-[1,1'-biphenyl]-4-amine. *Processes of Petrochemistry and Oil Refining*, 26(1), 97–106.